

## Supplementary Information for

### Pressure-stabilized graphenelike P layer in superconducting LaP<sub>2</sub>

Xing Li<sup>1†</sup>, Xiaohua Zhang<sup>1,2†</sup>, Zeng Yang<sup>3</sup>, Yong Liu<sup>1</sup>, and Guochun Yang<sup>1,2,\*</sup>

<sup>1</sup>*State Key Laboratory of Metastable Materials Science & Technology and Key Laboratory for Microstructural Material Physics of Hebei Province, School of Science, Yanshan University, Qinhuangdao 066004, China*

<sup>2</sup>*Centre for Advanced Optoelectronic Functional Materials Research and Key Laboratory for UV Light-Emitting Materials and Technology of Northeast Normal University, Changchun 130024, China*

<sup>3</sup>*High School Attached to Northeast Normal University, Changchun 130024, China*

<sup>†</sup>These authors contributed equally to this work.

\*Corresponding Authors E-mail: yanggc468@nenu.edu.cn; yanggc@ysu.edu.cn

<b>Index</b>	<b>Page</b>
1. Computational details .....	3
2. Phase stability and pressure-composition phase diagrams of various La-N/P/As compounds at 25, 50, 100, 200, and 300 GPa .....	6
3. Phonon dispersion curves of stable La-P phases .....	8
4. Crystal structures of stable La-P compounds .....	9
5. The PDOS of stable La-P compounds .....	10
6. The ELF maps of <i>P6/mmm</i> La <sub>0</sub> P <sub>2</sub> at 16 GPa and <i>Cmmm</i> La <sub>0</sub> P <sub>3</sub> at 50 GPa .....	10
7. The Fermi surfaces of LaP <sub>2</sub> at 16 GPa .....	11
8. The Fermi surfaces of MgB <sub>2</sub> at ambient pressure .....	12
9. The projected electronic band structures of 3p orbital of P atom and 5d (4f) orbital of La atom in LaP <sub>2</sub> at 16 GPa .....	13
10. Phonon dispersion curves of stable La-N phases .....	14
11. Phonon dispersion curves of stable La-As phases .....	15
12. Crystal structures of stable La-N compounds .....	16
13. The PDOS of stable La-N compounds .....	17
14. Crystal structures of stable La-As compounds .....	18
15. The PDOS of stable La-As compounds .....	19
16. The calculated EPC parameter ( $\lambda$ ), logarithmic average phonon frequency ( $\omega_{\log}$ ), and critical temperature of La-N/P/As compounds .....	20
17. Structural information of predicted stable La-N/P/As phases .....	21
18. References .....	25

## Computational Details

Our structural prediction approach is based on a global minimization of free energy surfaces merging ab initio total-energy calculations with CALYPSO (Crystal structure AnaLYsis by Particle Swarm Optimization) methodology as implemented in the CALYPSO code.<sup>1-2</sup> The structures of stoichiometry  $\text{La}_x\text{M}_y$  ( $x = 1, y = 0.5, 1, 1.5, 2, 3-8; x = 3, y = 4$ ; and  $M = \text{N, P, As}$ ) of La-N/P/As systems are searched with simulation cell sizes of 1-4 formula units (f.u.) at 1 atm and 25, 50, 100, 200 and 300 GPa. In the first step, random structures with certain symmetry are constructed in which atomic coordinates are generated by the crystallographic symmetry operations. Local optimizations<sup>3</sup> using the VASP code are done with the conjugate gradients method and stopped when enthalpy changes become smaller than  $1 \times 10^{-5}$  eV per cell. After processing the first generation structures, 60% of them with lower enthalpies are selected to construct the next generation structures by PSO (Particle Swarm Optimization). 40% of the structures in the new generation are randomly generated. A structure fingerprinting technique of bond characterization matrix is applied to the generated structures, so that identical structures are strictly forbidden. These procedures significantly enhance the diversity of the structures, which is crucial for structural global search efficiency. In most cases, structural searching simulations for each calculation were stopped after generating 1000 ~ 1200 structures (e.g., about 20 ~ 30 generations).

To further analyze the structures with higher accuracy, we select a number of structures with lower enthalpies and perform structural optimization using density functional theory within the generalized gradient approximation<sup>4</sup> as implemented in the VASP code. The cut-off energy for the expansion of wavefunctions into plane waves is set to 800 eV in all calculations, and the Monkhorst–Pack k-mesh with a maximum spacing of  $2\pi \times 0.03 \text{ \AA}^{-1}$  was individually adjusted in reciprocal space with respect to the size of each computational cell. This usually gives total energies well converged within  $\sim 1$  meV/atom. The electron-ion interaction is described by using all-electron projector augmented-wave method (PAW) with  $2s^22p^3, 3s^23p^3, 4s^24p^3$  and

$5s^25p^65d^16s^2$  considered as valence electrons for N, P, As, and La atom, respectively. The formation enthalpy ( $\Delta H$ ), relative to the element La and M, is calculated at each considered pressure according to the equation below:

$$\Delta H(\text{La}_x\text{M}_y) = [H(\text{La}_x\text{M}_y) - xH(\text{La}) - yH(\text{M})]/(x + y), \quad (1)$$

where  $H = U + PV$  is the enthalpy of each composition, and  $\Delta H$  is the formation enthalpy per atom of the given compound. Here,  $U$ ,  $P$ , and  $V$  are the internal energy, pressure, and volume, respectively. For clarity, the following phases for solid elements ( $P6_3/mmc$  and  $Fm-3m$  structure for La;<sup>5-6</sup> the  $Pa-3$ ,  $P4_12_12$ ,  $cg$ ,  $Pba2$  phases for N;<sup>7-8</sup> the I ( $Cmca$ ), VI ( $Pm-3m$ ), IV ( $Cmmm$ ), VII ( $P6/mmm$ ), and VIII ( $Im-3m$ ) phases for P;<sup>9</sup> and the I ( $R-3m$ ), II ( $Pm-3m$ ), III (monoclinic), and VI ( $Im-3m$ ) phases for As<sup>10</sup> were adopted.

The electron localization function (ELF) is used to describe and visualize chemical bonds of stable compounds.<sup>11</sup> The phonon dispersion curves and electron-phonon coupling (EPC) calculations are performed within the density functional perturbation theory (DFPT),<sup>12</sup> as implemented in the PHONOPY<sup>13</sup> and QUANTUM ESPRESSO<sup>14</sup> packages. We employ the ultrasoft pseudopotentials with  $2s^22p^3$ ,  $3s^23p^3$ ,  $4s^24p^3$ , and  $5s^25p^65d^16s^2$  considered as valence electrons for N, P, As, and La, respectively. The considered kinetic energy cutoff and Gaussians of width are 80 Ry and 0.02 Ry, respectively. To reliably calculate EPC in metallic systems, we need to sample dense k-meshes for electronic Brillouin zone integration and enough q-meshes for evaluating average contributions from the phonon modes. Dependent on specific structures of stable compounds, different k-meshes and q-meshes are used:  $16 \times 16 \times 16$  k-meshes and  $4 \times 4 \times 4$  q-meshes for LaN in the  $Pm-3m$  structure,  $12 \times 12 \times 19$  k-meshes and  $4 \times 4 \times 3$  q-meshes for La<sub>2</sub>P in the  $Cmcm$  structure,  $9 \times 9 \times 15$  k-meshes and  $3 \times 3 \times 5$  q-meshes for LaP in the  $P4/nmm$  structure,  $12 \times 12 \times 15$  k-meshes and  $4 \times 4 \times 5$  q-meshes for LaP in the  $Cmmm$  structure,  $12 \times 8 \times 4$  k-meshes and  $6 \times 4 \times 2$  q-meshes for LaP in the  $Imma$  structure,  $12 \times 12 \times 12$  k-meshes and  $4 \times 4 \times 4$  q-meshes for La<sub>2</sub>P<sub>3</sub> in the  $Cmmm$  structure,  $16 \times 16 \times 16$  k-meshes and  $4 \times 4 \times 4$  q-meshes for LaP<sub>2</sub> in the  $P6/mmm$  structure,  $16 \times 16 \times 16$  k-meshes and  $4 \times 4 \times 4$  q-meshes for LaP<sub>2</sub> in the  $Fd-3m$  structure,  $9 \times 9 \times 15$  k-meshes and  $3 \times 3 \times 5$  q-meshes

for LaAs in the  $P4/nmm$  structure,  $8 \times 8 \times 8$  k-meshes and  $4 \times 4 \times 4$  q-meshes for LaAs<sub>3</sub> in the  $Im-3$  structure,  $12 \times 12 \times 12$  k-meshes and  $4 \times 4 \times 4$  q-meshes for LaAs<sub>3</sub> in the  $Pm-3m$  structure. we have calculated the superconducting  $T_c$  of the La-N/P/As phases as estimated from the Allen-Dynes modified McMillan equation:<sup>15</sup>

$$T_c = \frac{\omega_{log}}{1.2} \exp \left[ - \frac{1.04(1 + \lambda)}{\lambda - \mu^* (1 + 0.62\lambda)} \right]. \quad (2)$$

Here,  $\mu^*$  is the Coulomb pseudopotential ( $\mu^* = 0.1$ ). The EPC parameter,  $\lambda$ , and the logarithmic average phonon frequency,  $\omega_{log}$ , are calculated by the Eliashberg spectral function for electron-phonon interaction:

$$\alpha^2 F(\omega) = \frac{1}{N(E_F)} \sum_{kq,v} |g_{k,k+q,v}|^2 \delta(\varepsilon_k) \delta(\varepsilon_{k+q}) \delta(\omega - \omega_{q,v}) \quad (3)$$

where  $\lambda = 2 \int d\omega \frac{\alpha^2 F(\omega)}{\omega}$ ;  $\omega_{log} = \exp \left[ \frac{2}{\lambda} \int \frac{d\omega}{\omega} \alpha^2 F(\omega) \ln(\omega) \right]$ . Herein,  $N(E_F)$  is the electron density of states at the Fermi level,  $\omega_{q,v}$  is the phonon frequency of mode  $v$  and wave vector  $q$ , and  $|g_{k,k+q,v}|$  is the electron-phonon matrix element between two electronic states with momenta  $k$  and  $k + q$  at the Fermi level.<sup>16-17</sup>

## Supplementary Figures

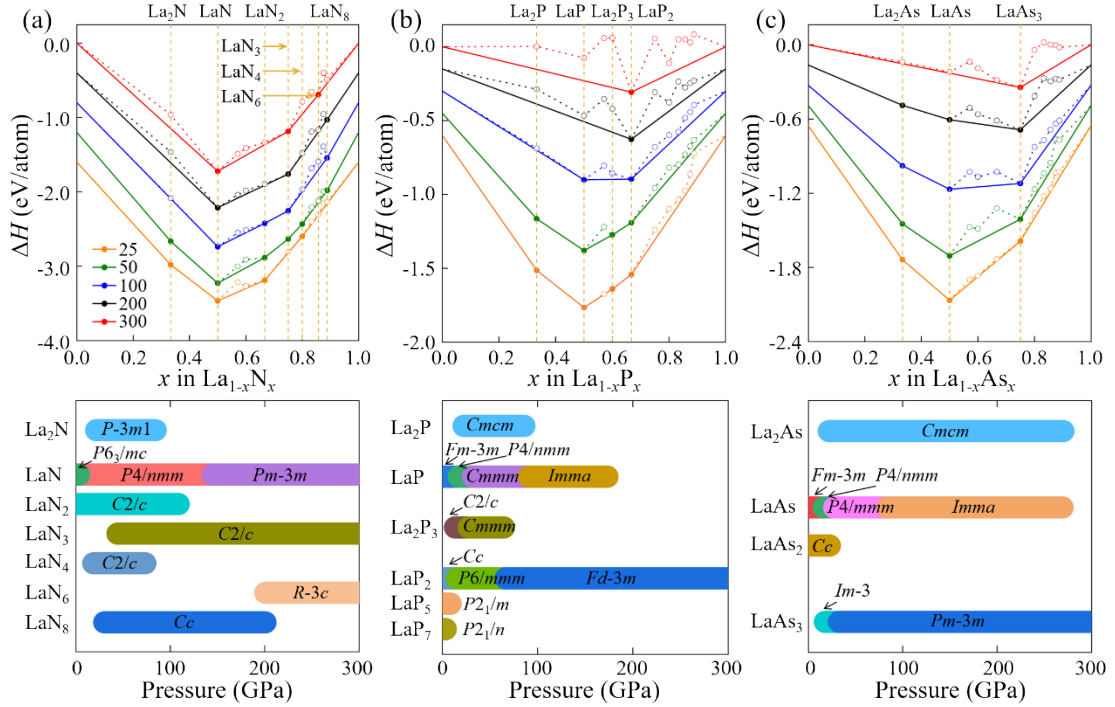


**Fig. S1.** Phase stability and pressure-composition phase diagrams of various La-N/P/As compounds at 25, 50, 100, 200, and 300 GPa. (a) La-N system, (b) La-P system, and (c) La-As system. For clarity, we have offset the formation enthalpy diagrams in the La-N/P/As systems by -0.4, -0.15, and -0.15 eV for each considered pressure (except 25 GPa), respectively. Generally, the phases lying on the solid lines of the convex hull are thermodynamically stable. However, the rest phases that sitting on the dotted lines of the convex hull are unstable or metastable.

By calculating the enthalpy difference of adjacent stable components, the pressure-composition phase diagram is determined. For the La-N system, the wurtzite (B4)  $\text{LaN}^{18}$  and  $\text{ThC}_2$ -type  $\text{LaN}_2^{19}$  that stabilize at 1 atm have been reproduced. With increasing pressure, a phase transition for  $\text{LaN}$  is first found from B4 phase to  $P4/nmm$  phase at 3.3 GPa, which is the same phase found experimentally at 22.6 GPa,<sup>20</sup> and then it becomes reported CsCl (B2) phase at 145 GPa.<sup>21</sup> As for the  $\text{ThC}_2$ -type  $\text{LaN}_2^{19}$  that stabilizes at ambient pressure, it maintains stable to 109 GPa, and there is no phase transition at higher pressure. Besides, four N-rich nitrides  $\text{LaN}_3$ ,  $\text{LaN}_4$ ,  $\text{LaN}_6$ ,  $\text{LaN}_8$  and one La-rich  $\text{La}_2\text{N}$  become stable in the range of 44-300 GPa, 18.4-73.7 GPa, 200.6-300 GPa, 30.1-200.8 GPa, and 21.6-84.7 GPa, respectively.

For the La-P system, in addition to readily reproducing the already known NaCl-type (B1)  $\text{LaP}$ ,<sup>22</sup>  $Cc$   $\text{LaP}_2$ ,<sup>23</sup>  $P2_1/m$   $\text{LaP}_5$ ,<sup>24</sup> and  $P2_1/n$   $\text{LaP}_7$ <sup>25</sup> at 1 atm and the theoretically proposed high-pressure  $Imma$   $\text{LaP}$  phase,<sup>26</sup> we identify several thermodynamically stable chemical compositions (e.g.  $\text{La}_2\text{P}$ ,  $\text{LaP}$ ,  $\text{La}_2\text{P}_3$ , and  $\text{LaP}_2$ ) at

high pressures. The NaCl-type (B1) LaP,<sup>22</sup> *Cc* LaP<sub>2</sub>,<sup>23</sup> *P2<sub>1</sub>/m* LaP<sub>5</sub>,<sup>24</sup> and *P2<sub>1</sub>/n* LaP<sub>7</sub><sup>25</sup> are stabilized to 17.2 GPa, 15.4 GPa, 8.7 GPa and 3.5 GPa, respectively. At higher pressures, LaP exists in three different high-pressure phases *P4/nmm* (17.2-32.1 GPa), *Cmmm* (32.1-91.2 GPa), and *Imma* (91.2-173.4 GPa),<sup>26</sup> while LaP<sub>2</sub> adopts *P6/mmm* and *Fd-3m* symmetry when the pressure is greater than 15.4 GPa and 66.6 GPa, respectively. Besides, two hitherto unknown stoichiometries, P-rich La<sub>2</sub>P<sub>3</sub> and La-rich La<sub>2</sub>P, emerge as being stable. The former exists with the symmetry of *C2/c* (13.4-27.8 GPa) and *Cmmm* (27.8-64.6 GPa). The latter adopts the *Cmcm* space group at 22.5-86.1 GPa.

For the La-As system, the B1-phase LaAs<sup>27</sup> and *Cc* LaAs<sub>2</sub><sup>23</sup> that stabilize at 1 atm have also been discovered. *Cc* LaAs<sub>2</sub> is stable to 22.9 GPa and there is no phase transition, while LaAs has three high-pressure phases *P4/nmm* (16.2-27.5 GPa), *P4/mmm* (27.5-84 GPa), and *Imma* (84-269.5 GPa), where *P4/mmm* and *Imma* phases consistent with previously reported.<sup>26</sup> La-rich *Cmcm* La<sub>2</sub>As is stable within 21.7-270.2 GPa and is isostructural to La<sub>2</sub>P. The As-rich LaAs<sub>3</sub> is stable with *Im-3* space group at 17.6 GPa, and it undergoes a phase transition to Cu<sub>3</sub>Au-type phase (*Pm-3m* symmetry) at 32.5 GPa.

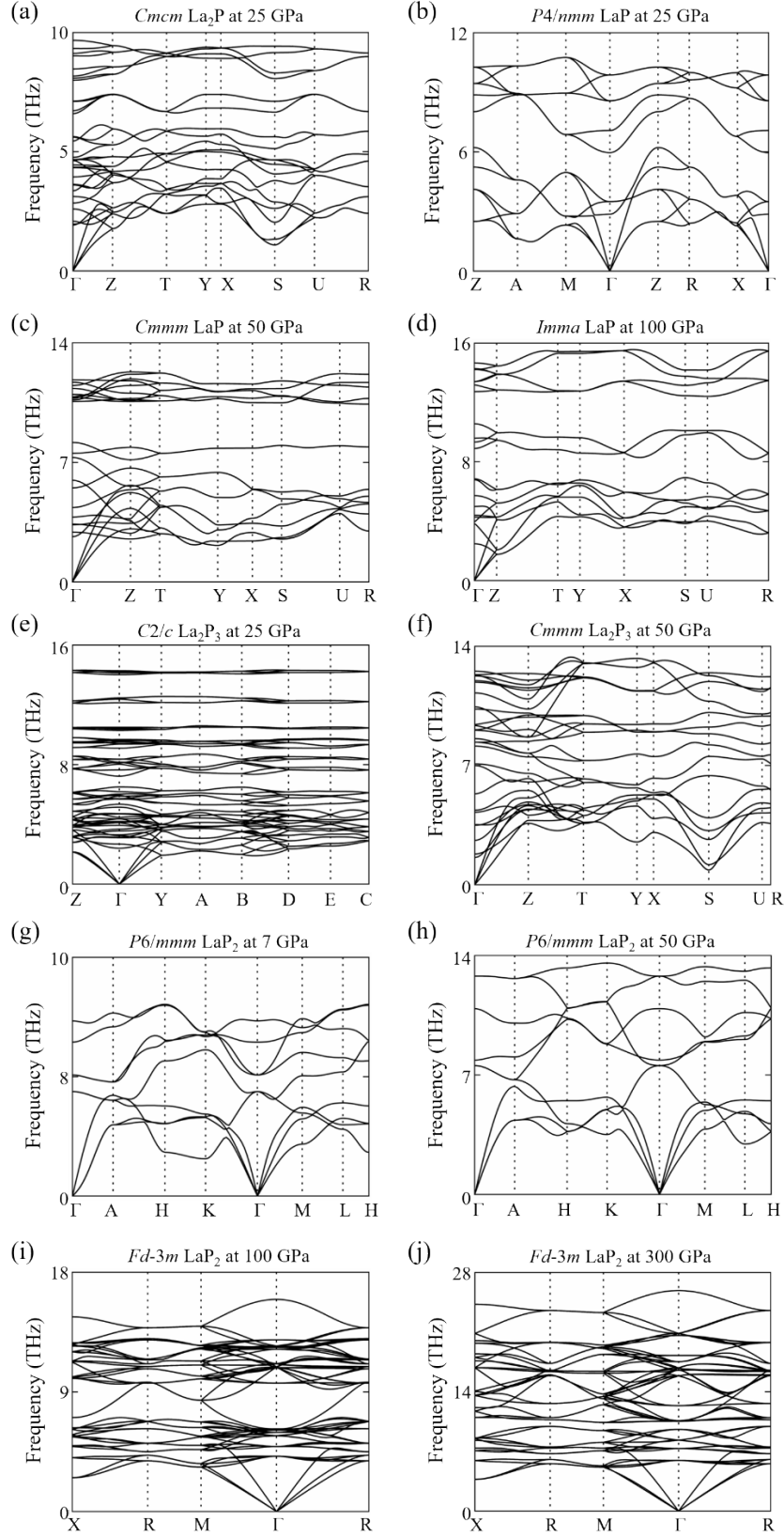


**Fig. S2.** Phonon dispersion curves of stable La-P phases. The absence of imaginary frequency in the whole Brillouin zone indicates these structures are dynamically stable. Note that  $\text{LaP}_2$  has a positive formation enthalpy of 50 meV/atom at 7 GPa,<sup>28</sup> which meets the criterion of metastable phase.

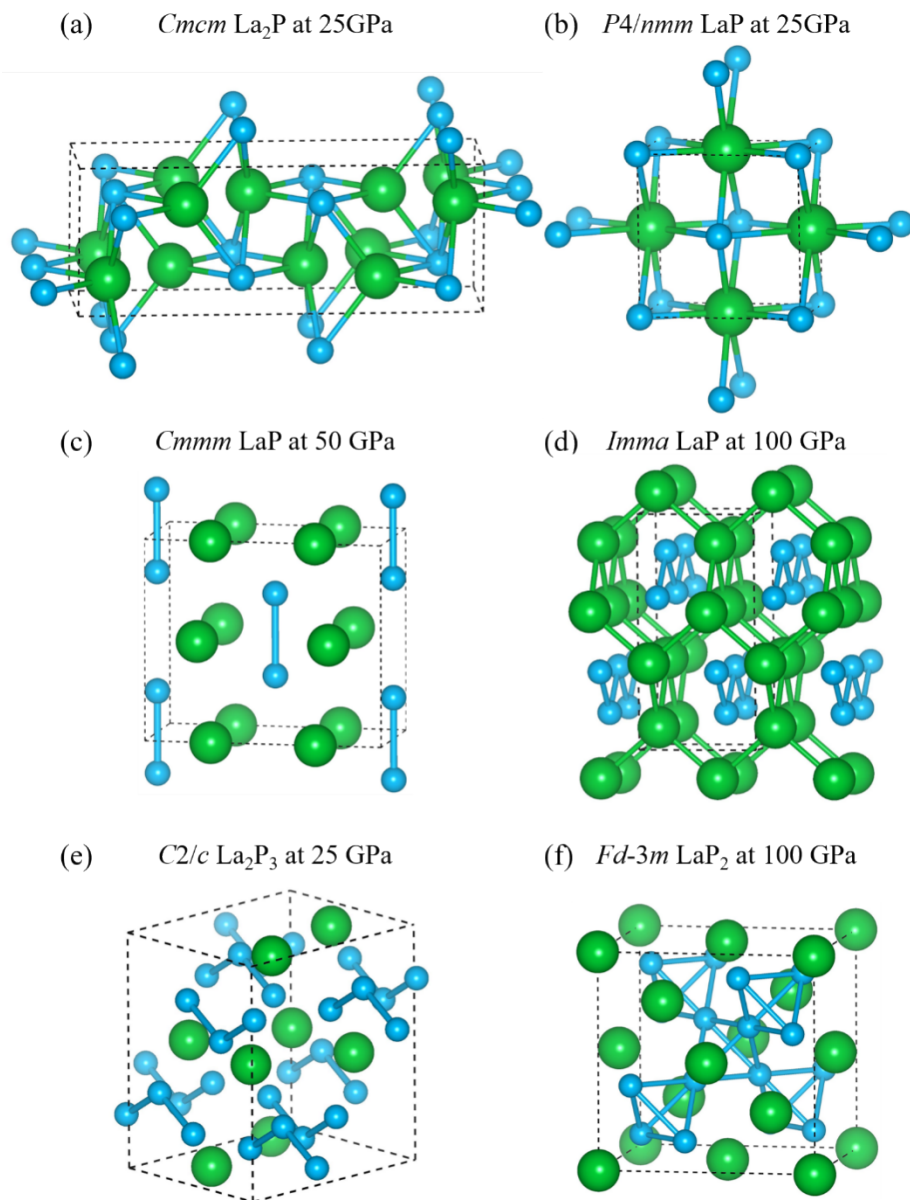


**Fig. S3.** Crystal structures of stable La-P compounds, the big and small balls represent La and P atoms, respectively.

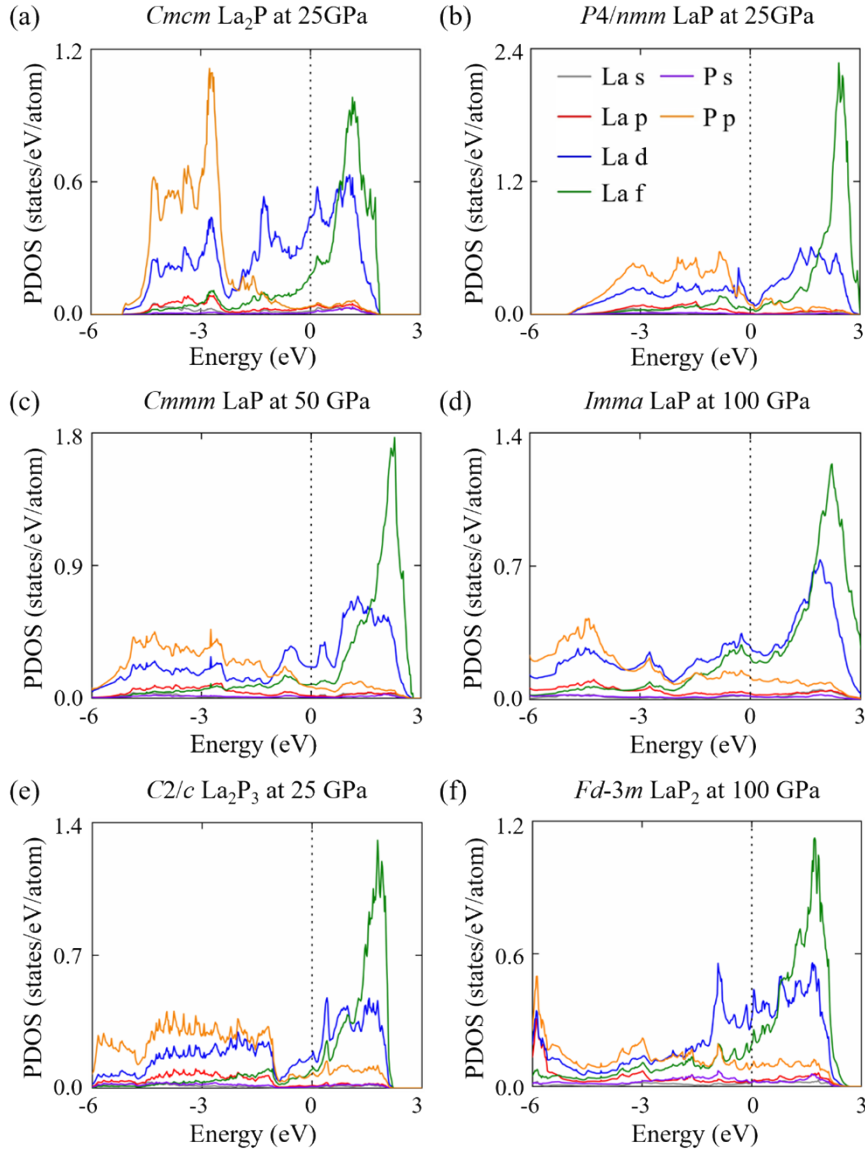


**Fig. S4.** The projected electron density of states (PDOS) of stable La-P compounds.

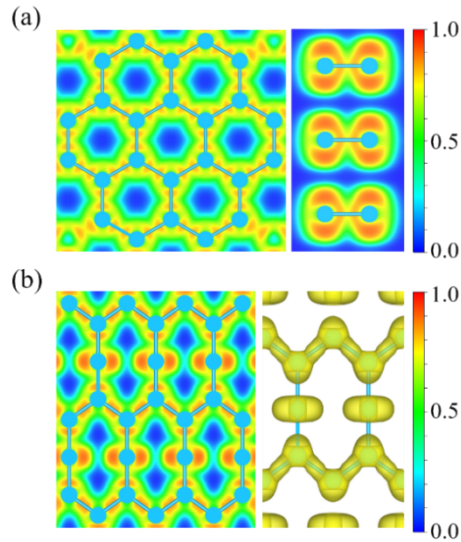


**Fig. S5.** The ELF maps and isosurface with the value of 0.7 of (a)  $P6/mmm$   $\text{La}_0\text{P}_2$  at 16 GPa and (b)  $Cmmm$   $\text{La}_0\text{P}_3$  at 50 GPa.

For  $\text{LaP}_2$ , Bader charge analysis<sup>29</sup> shows that each P atom accepts  $0.70e^-$  from La atom. Besides three electrons of each P atom are used to form covalent bonds via  $sp^2$  hybridization, the left electrons occupy P-P antibonding orbitals and appear in the form of lone electron pairs, respectively. The former weakens the P-P bonds, in consistent with the enhancement of localized electrons of P-P bonds after removing La atoms from  $\text{LaP}_2$  and the bonding length analysis. For  $\text{La}_2\text{P}_3$ , the obtained charges of  $\text{P}_1$  and  $\text{P}_2$  atoms are  $0.72e^-$  and  $0.87e^-$ , respectively, and the localized electrons of the P-P bond are also enhanced after removing the La atoms.

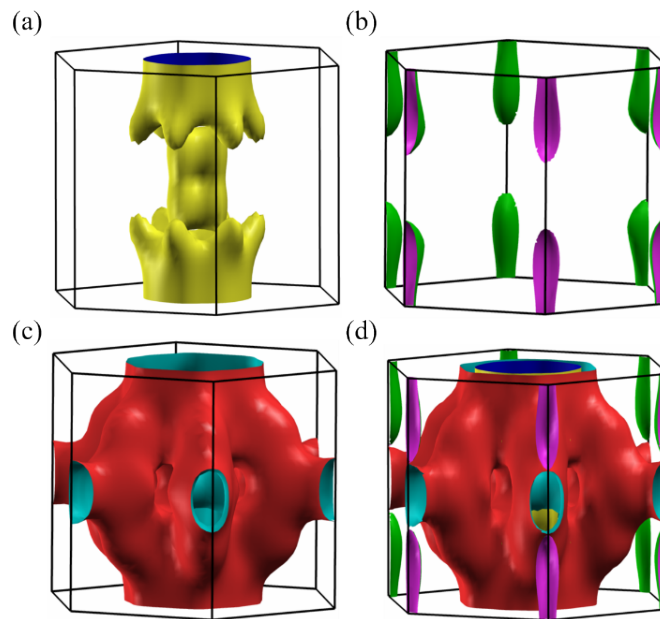


**Fig. S6.** (a-c) The Fermi surfaces associated to bands crossing the Fermi energy of  $\text{LaP}_2$  at 16 GPa, and (d) the side view of merged Fermi surfaces.

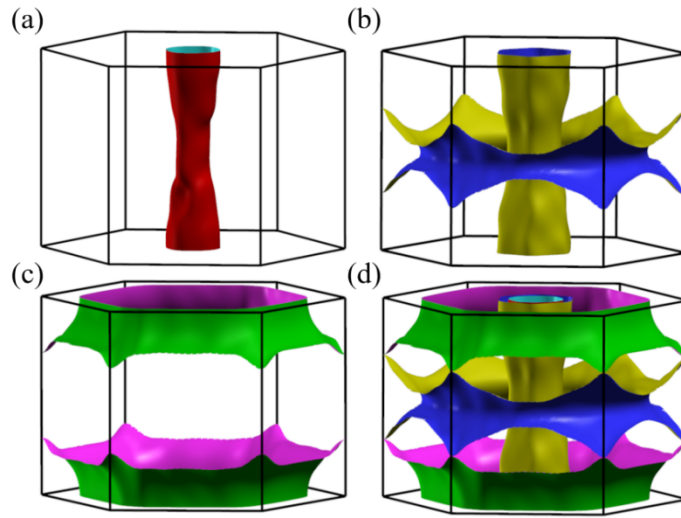


**Fig. S7.** (a-c) The Fermi surfaces associated to bands crossing the Fermi energy of  $\text{MgB}_2$ , and (d) the side view of the merged Fermi surface. They are the same as the Fermi surfaces of  $\text{MgB}_2$  shown in the literature,<sup>30</sup> except that the selected periodic unit is different.

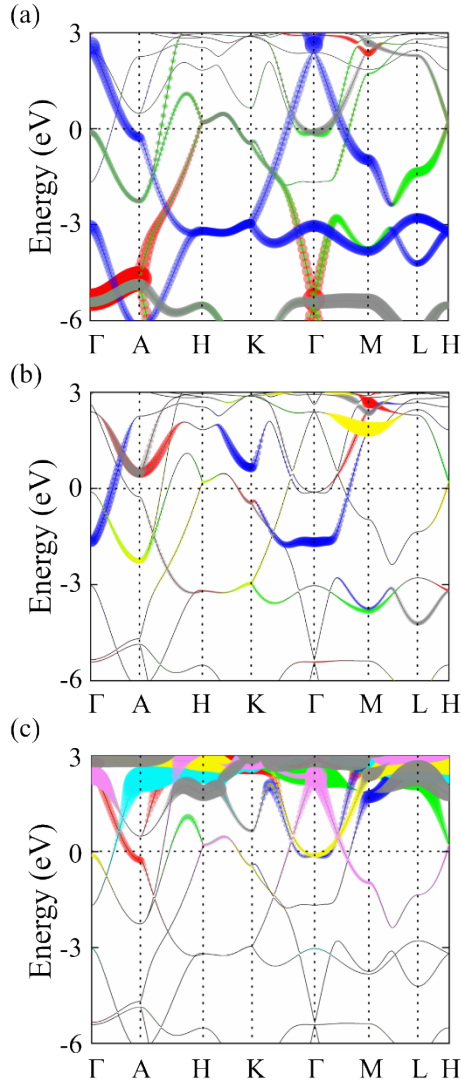


**Fig. S8.** The projected electronic band structures of (a) 3p orbital of P atom, (b) 5d orbital of La atom, and (c) 4f orbital of La atom in  $\text{LaP}_2$  at 16 GPa. For (a), red, green, blue, and gray represent 3s,  $3p_y$ ,  $3p_z$  and  $3p_x$  orbitals of P atom, respectively; for (b), red, green, blue, yellow and gray represent the  $5d_{xy}$ ,  $5d_{yz}$ ,  $5d_{z^2}$ ,  $5d_{xz}$  and  $5d_{x^2-y^2}$  orbitals of La atom, respectively; and for (c), red, green, blue, cyan, yellow, magenta and gray represent the  $4f_{y(3x^2-y^2)}$ ,  $4f_{xyz}$ ,  $4f_{yz^2}$ ,  $4f_{z^3}$ ,  $4f_{xz^2}$ ,  $4f_{z(x^2-y^2)}$ , and  $4f_{x(x^2-3y^2)}$  orbitals of La atom, respectively.

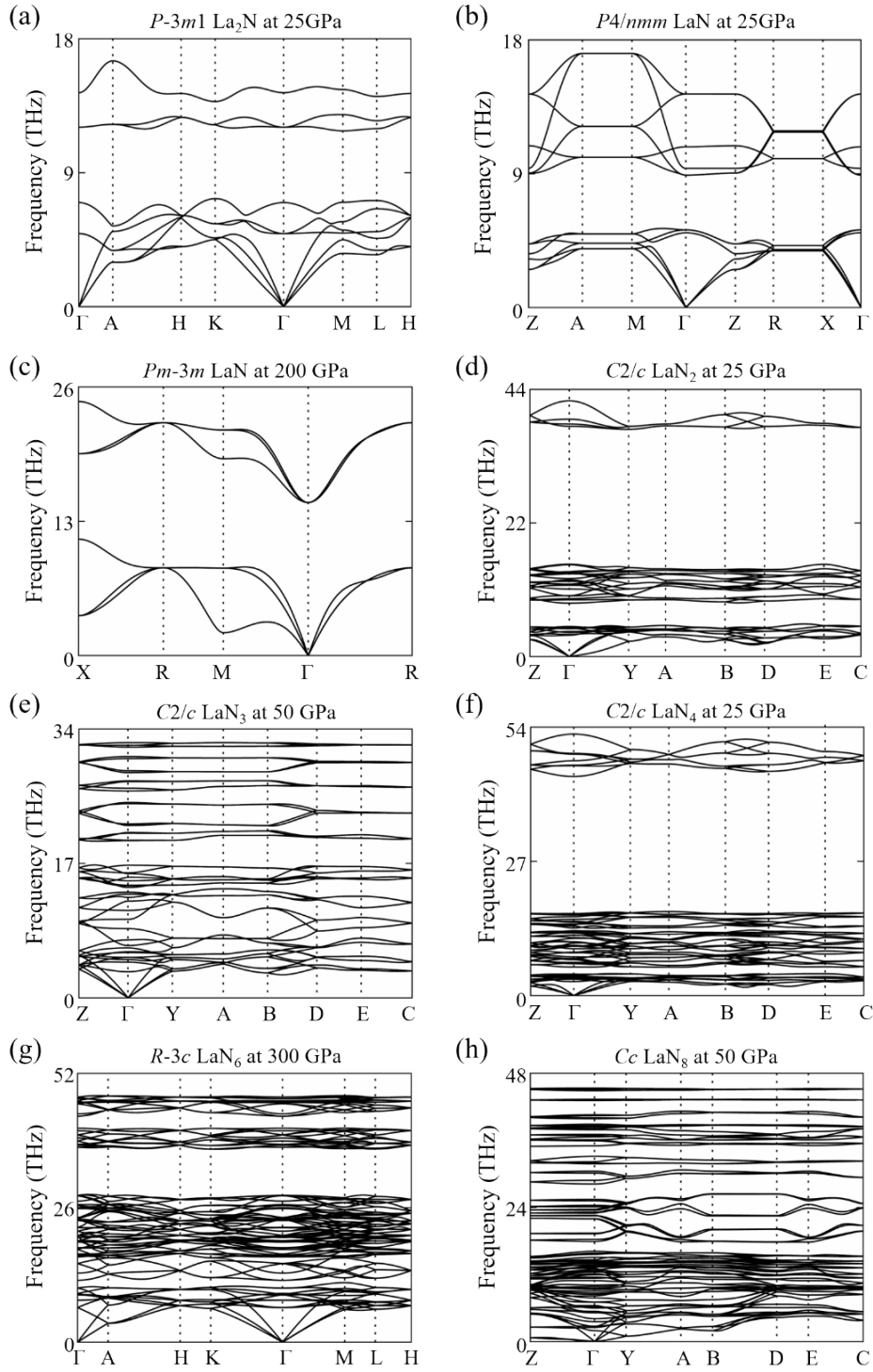


**Fig. S9.** Phonon dispersion curves of stable La-N phases.

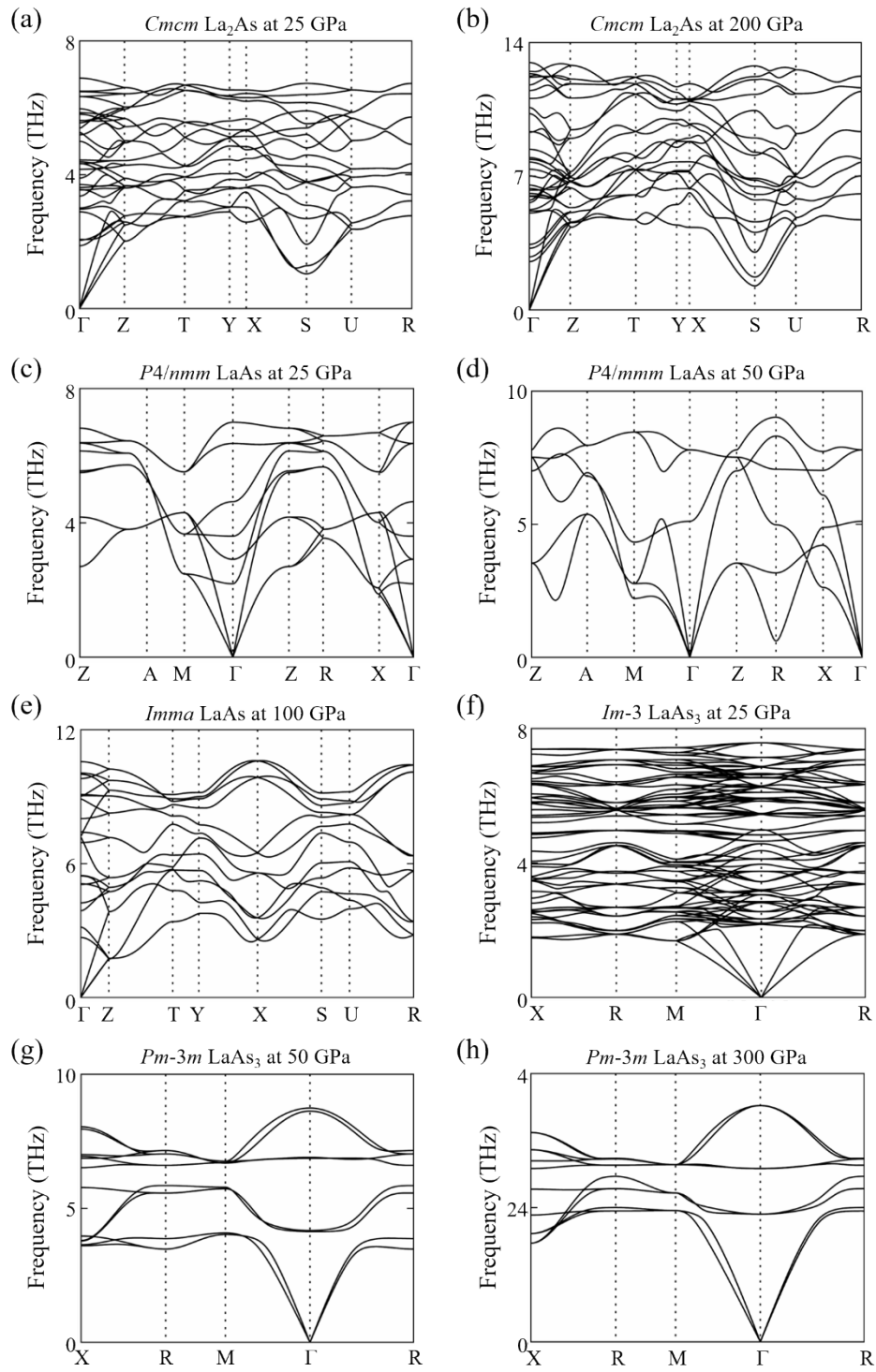
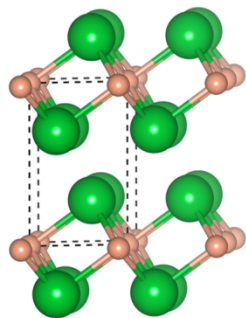
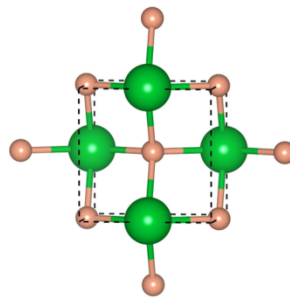


**Fig. S10.** Phonon dispersion curves of stable La-As phases.

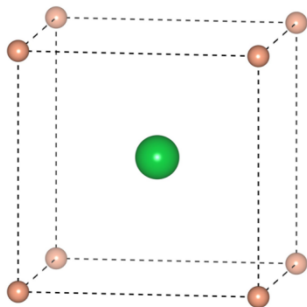
(a)  $P-3m1$   $\text{La}_2\text{N}$  at 25GPa



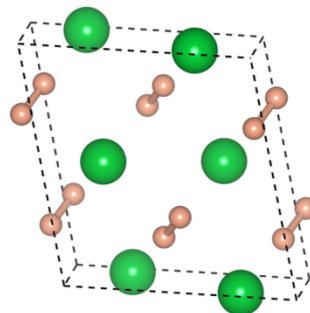
(b)  $P4/nmm$   $\text{LaN}$  at 25GPa



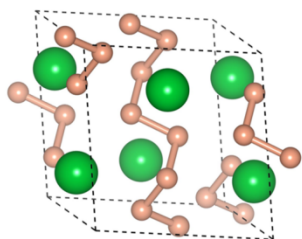
(c)  $Pm-3m$   $\text{LaN}$  at 200 GPa



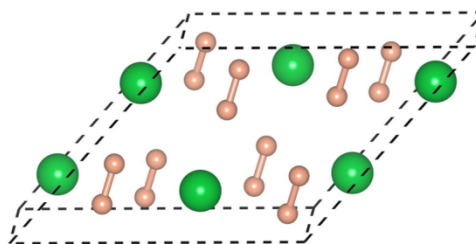
(d)  $C2/c$   $\text{LaN}_2$  at 25 GPa



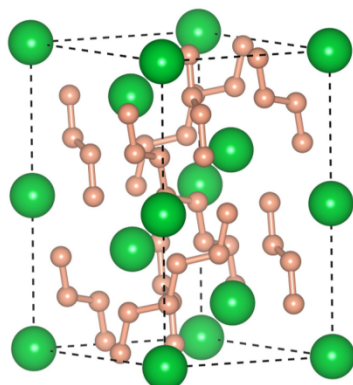
(e)  $C2/c$   $\text{LaN}_3$  at 50 GPa



(f)  $C2/c$   $\text{LaN}_4$  at 25 GPa



(g)  $R-3c$   $\text{LaN}_6$  at 300 GPa



(h)  $Cc$   $\text{LaN}_8$  at 200 GPa

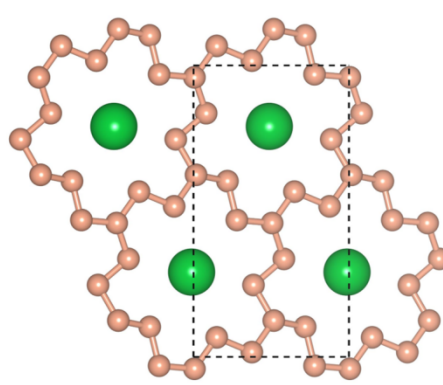


**Fig. S11.** Crystal structures of stable La-N compounds, the big and small balls represent La and N atoms, respectively.

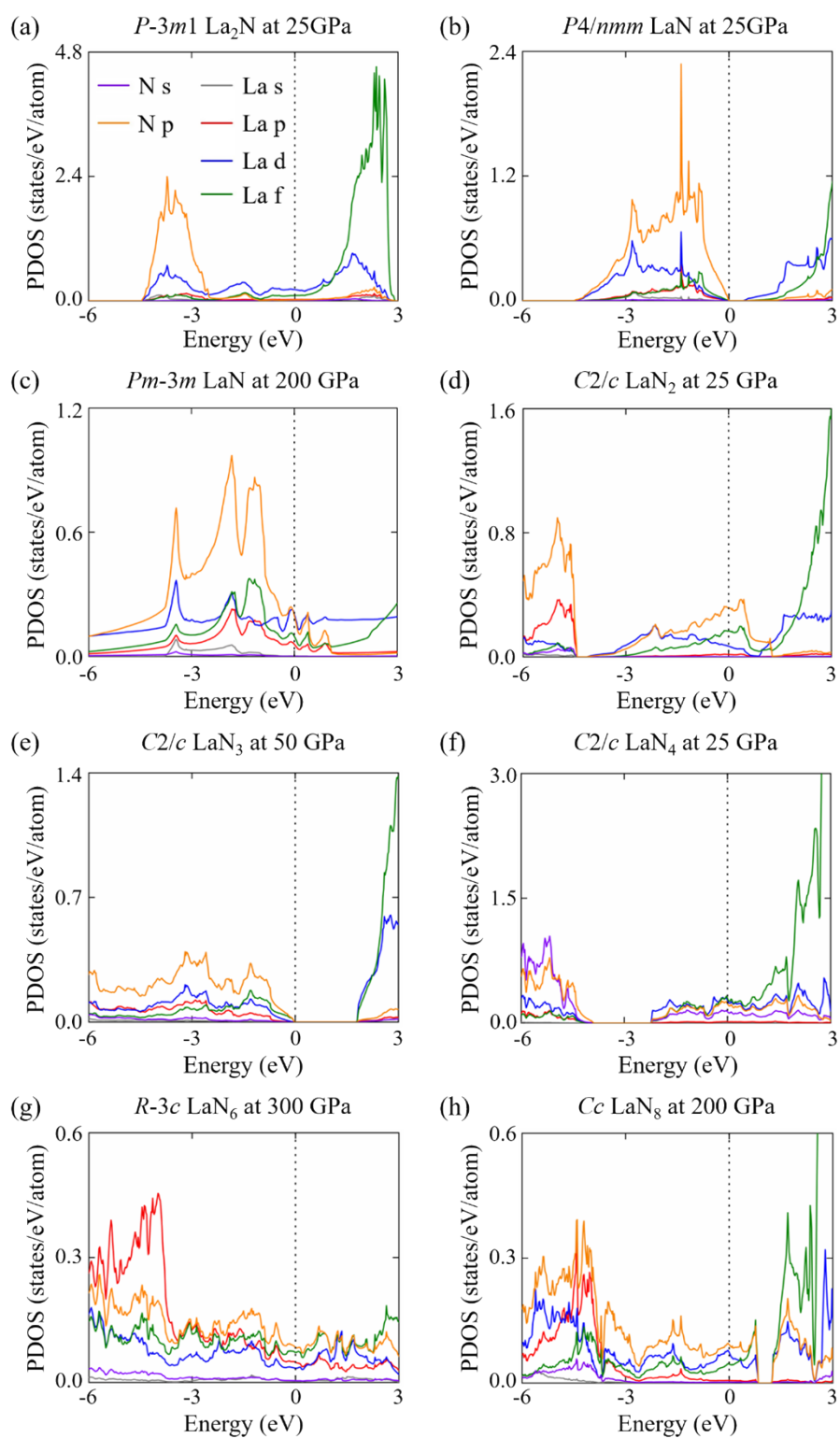


**Fig. S12.** The PDOS of stable La-N compounds.

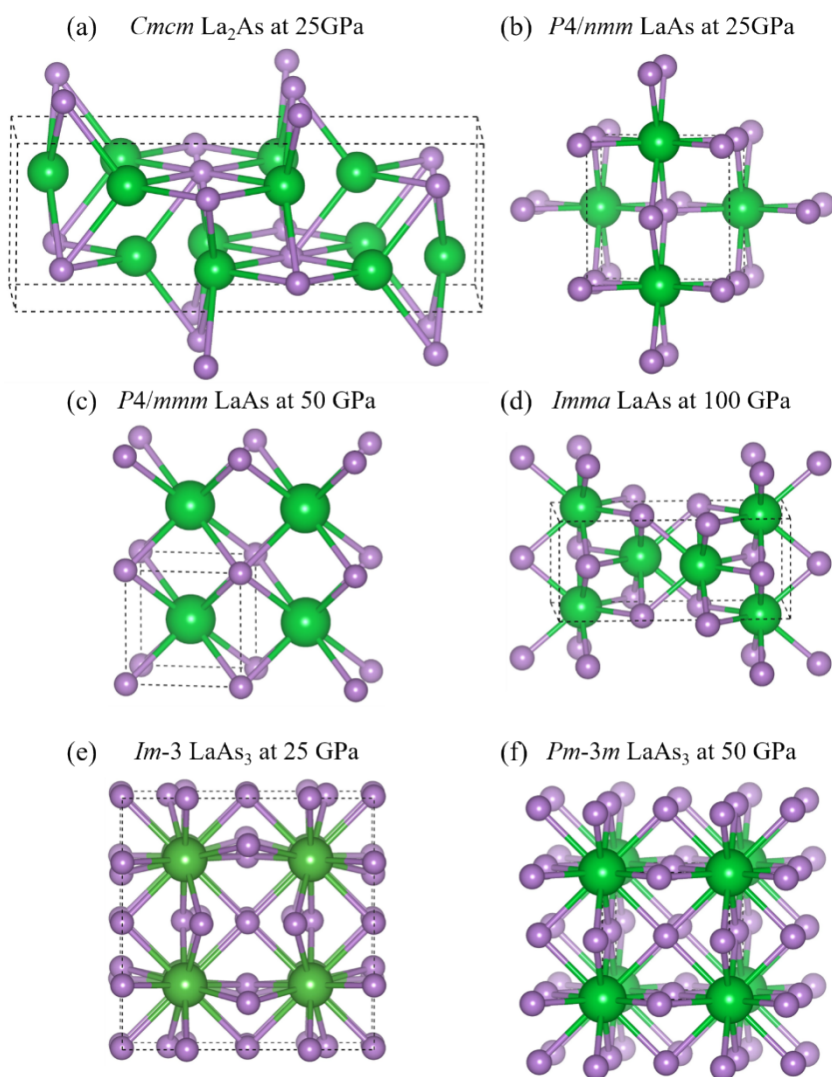


**Fig. S13.** Crystal structures of stable La-As compounds, the big and small balls represent La and As atoms, respectively.

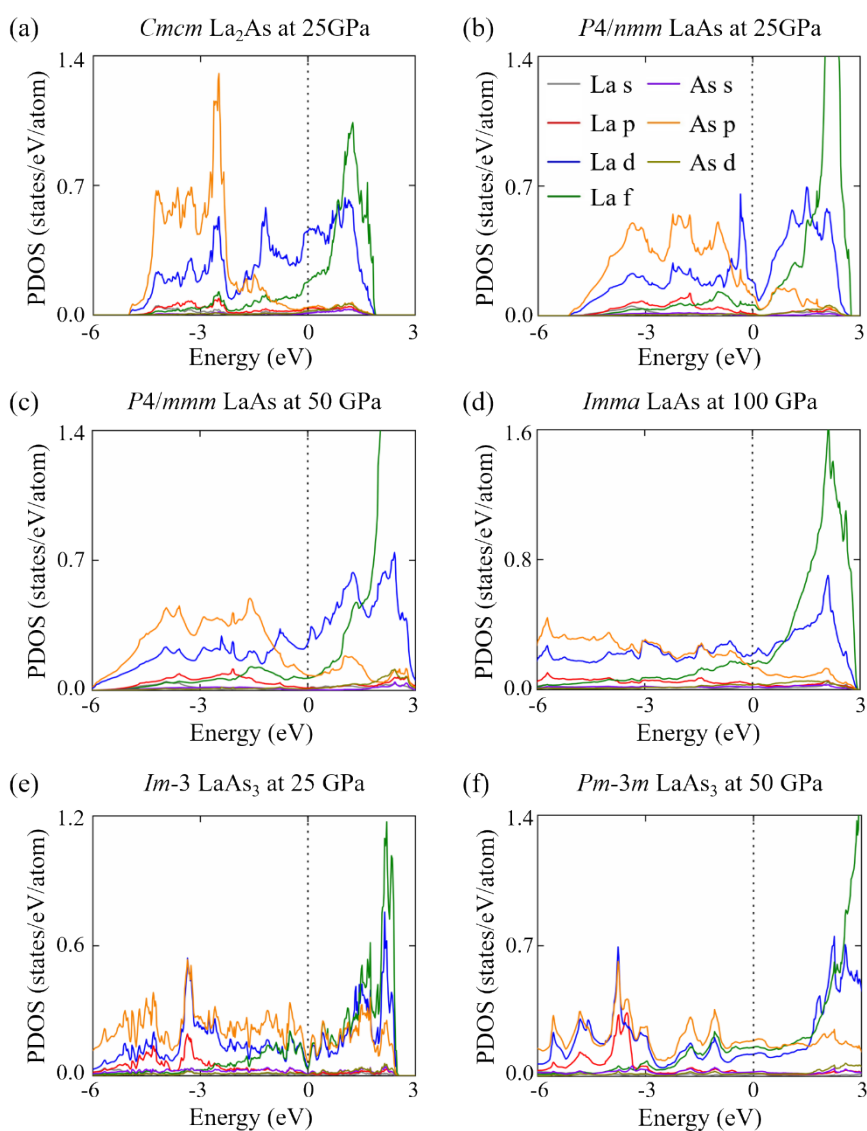


**Fig. S14.** The PDOS of stable La-As compounds.

## Supplementary Tables

**Table S1.** The calculated EPC parameter ( $\lambda$ ), logarithmic average phonon frequency ( $\omega_{\log}$ ), critical temperature with  $\mu^* = 0.10$  of several predicted stable La-N/P/As phases.

Phases	Pressure (GPa)	$\lambda$	$\omega_{\log}$ (K)	$T_c$ (K)
<i>Pm-3m</i> LaN	200	0.47	334.28	3.27
<i>Cmcm</i> La <sub>2</sub> P	25	0.56	163.89	3.01
<i>P4/nmm</i> LaP	25	0.48	154.38	1.56
<i>Cmmm</i> LaP	50	0.58	168.19	3.56
<i>Imma</i> LaP	100	0.45	296.75	2.18
<i>Cmmm</i> La <sub>2</sub> P <sub>3</sub>	50	0.58	285.75	5.77
<i>Fd-3m</i> LaP <sub>2</sub>	100	0.51	358.45	4.56
	300	0.32	501.68	0.45
<i>P4/nmm</i> LaAs	25	0.42	124.48	0.72
<i>Im-3</i> LaAs <sub>3</sub>	25	0.66	138.55	4.18
<i>Pm-3m</i> LaAs <sub>3</sub>	32.5	0.85	121.80	6.36
	50	0.66	138.32	4.19
	100	0.41	219.66	1.01
	200	0.26	329.58	0.03

**Table S2.** Structural information of the predicted stable La-N/P/As phases.

Phases	Pressure (GPa)	Lattice Parameters (Å, °)	Wyckoff Positions (fractional)			
			atoms	x	y	z
<i>P-3m1</i> La <sub>2</sub> N	25	a=3.3937	La(2d)	0.3333	0.6667	0.2823
		b=3.3937	N(1a)	0.0000	0.0000	0.0000
		c=5.1180				
		α=90.0000				
		β=90.0000				
<i>P4/nmm</i> LaN	25	a=4.2239	La(2c)	0.0000	0.5000	0.1741
		b=4.2239	N(2b)	0.0000	0.0000	0.5000
		c=3.2484				
		α=90.0000				
		β=90.0000				
<i>Pm-3m</i> LaN	200	a=2.6425	La(1b)	0.5000	0.5000	0.5000
		b=2.6425	N(1a)	0.0000	0.0000	0.0000
		c=2.6425				
		α=90.0000				
		β=90.0000				
<i>C2/c</i> LaN <sub>2</sub>	25	a=6.4755	La(8f)	0.5000	0.6812	0.2500
		b=3.9176	N(4e)	0.1947	0.6248	0.4476
		c=6.0795				
		α=90.0000				
		β=103.5621				
<i>C2/c</i> LaN <sub>3</sub>	50	a=5.0426	La(4e)	0.0000	0.6620	0.7500
		b=5.7257	N(4e)	0.0000	0.2001	0.7500
		c=5.2213	N(8f)	0.8855	0.9517	0.0468
		α=90.0000				
		β=98.7623				
<i>C2/c</i> LaN <sub>4</sub>	25	a=8.4135	La(4e)	0.0000	0.4096	0.2500
		b=4.3370	N(8f)	0.2936	0.3888	0.1798
		c=7.5407	N(8f)	0.1311	0.1501	0.6198
		α=90.0000				
		β=131.0734				
<i>R-3c</i> LaN <sub>6</sub>	300	a=5.2932	La(6b)	0.0000	0.0000	0.0000
		b=5.2932	N(32f)	0.7780	0.0292	0.6833
		c=9.3401				
		α=90.0000				

		$\beta=90.0000$				
		$\gamma=120.0000$				
<i>Cc</i> LaN <sub>8</sub>	200	a=5.4790	La(4a)	0.9878	0.7092	0.0130
		b=9.2867	N(4a)	0.0059	0.9592	0.5457
		c=4.5657	N(4a)	0.0165	0.6246	0.5701
		$\alpha=90.0000$	N(4a)	0.8861	0.2534	0.9660
		$\beta=115.1229$	N(4a)	0.7185	0.8970	0.0037
		$\gamma=90.0000$	N(4a)	0.3755	0.9836	0.0788
			N(4a)	0.0817	0.1639	0.0066
			N(4a)	0.7788	0.0304	0.0466
			N(4a)	0.1493	0.9331	0.0602
<i>Cmcm</i> La <sub>2</sub> P	25	a=3.6413	La(4c)	0.0000	0.0707	0.2500
		b=13.2916	La(4c)	0.5000	0.2379	0.2500
		c=4.9514	P(4c)	0.5000	0.0983	0.7500
		$\alpha=90.0000$				
		$\beta=90.0000$				
		$\gamma=90.0000$				
<i>P4/nmm</i> LaP	25	a=4.9262	La(2c)	0.0000	0.5000	0.4143
		b=4.9262	P(2a)	0.0000	0.0000	0.0000
		c=3.1840				
		$\alpha=90.0000$				
		$\beta=90.0000$				
		$\gamma=90.0000$				
<i>Cmmm</i> LaP	50	a=6.7801	La(4g)	0.7214	0.0000	0.0000
		b=5.7164	P(4j)	0.0000	0.7965	0.5000
		c=3.4034				
		$\alpha=90.0000$				
		$\beta=90.0000$				
		$\gamma=90.0000$				
<i>Imma</i> LaP	100	a=3.0510	La(4e)	0.5000	0.7500	0.1089
		b=4.2290	P(4e)	0.0000	1.2500	0.1576
		c=8.3695				
		$\alpha=90.0000$				
		$\beta=90.0000$				
		$\gamma=90.0000$				
<i>C2/c</i> La <sub>2</sub> P <sub>3</sub>	25	a=8.3636	La(8f)	0.2337	0.0163	-0.1409
		b=7.0176	P(8f)	0.0092	0.2219	0.4676
		c=6.8528	P(4e)	0.0000	0.3551	-0.2500
		$\alpha=90.0000$				
		$\beta=113.0578$				
		$\gamma=90.0000$				
<i>Cmmm</i> La <sub>2</sub> P <sub>3</sub>	50	a=3.5790	La(4i)	0.0000	0.8799	0.0000
		b=11.8726	P(2c)	0.5000	0.0000	0.5000

		c=3.6893 $\alpha=90.0000$ $\beta=90.0000$ $\gamma=90.0000$	P(4j)	0.5000	0.1966	0.5000
<i>P6/mmm</i> LaP <sub>2</sub>	25	a=3.9383 b=3.9383 c=3.8107 $\alpha=90.0000$ $\beta=90.0000$ $\gamma=120.0000$	La(1a) P(2d)	0.0000 0.6667	0.0000 0.3333	0.0000 0.3333
<i>Fd-3m</i> LaP <sub>2</sub>	100	a=6.6083 b=6.6083 c=6.6083 $\alpha=90.0000$ $\beta=90.0000$ $\gamma=90.0000$	La(8b) P(16c)	0.5000 0.6250	0.5000 0.3750	0.5000 0.8750
<i>Cmcm</i> La <sub>2</sub> As	25	a=3.7110 b=13.5411 c=4.9948 $\alpha=90.0000$ $\beta=90.0000$ $\gamma=90.0000$	La(4c) La(4c) As(4c)	0.5000 0.0000 0.0000	0.0733 0.7639 0.9026	1.2500 0.7500 1.2500
<i>P4/nmm</i> LaAs	25	a=5.1194 b=5.1194 c=3.1436 $\alpha=90.0000$ $\beta=90.0000$ $\gamma=90.0000$	La(2c) As(2b)	0.0000 0.0000	0.5000 0.0000	0.9287 0.5000
<i>P4/mmm</i> LaAs	50	a=3.5036 b=3.5036 c=2.9318 $\alpha=90.0000$ $\beta=90.0000$ $\gamma=90.0000$	La(1d) As(1a)	0.5000 0.0000	0.5000 0.0000	0.5000 0.0000
<i>Imma</i> LaAs	100	a=3.5961 b=4.0537 c=8.1957 $\alpha=90.0000$ $\beta=90.0000$ $\gamma=90.0000$	La(4e) As(4e)	0.0000 0.5000	-0.2500 0.2500	0.1215 0.1329
<i>Im-3</i> LaAs <sub>3</sub>	25	a=8.3424 b=8.3424 c=8.3424	La(8c) As(12d) As(12e)	0.2500 0.7443 0.1864	0.2500 0.0000 0.0000	0.2500 0.0000 0.5000

		$\alpha=90.0000$				
		$\beta=90.0000$				
		$\gamma=90.0000$				
<i>Pm-3m</i> LaAs <sub>3</sub>	50	a=3.9852	La(1a)	0.0000	0.0000	0.0000
		b=3.9852	As(3c)	0.5000	0.5000	0.0000
		c=3.9852				
		$\alpha=90.0000$				
		$\beta=90.0000$				
		$\gamma=90.0000$				

## References

- 1 Y. Wang, J. Lv, L. Zhu and Y. Ma, *Comput. Phys. Commun.*, 2012, **183**, 2063-2070.
- 2 Y. Wang, J. Lv, L. Zhu and Y. Ma, *Phys. Rev. B*, 2010, **82**, 094116.
- 3 G. Kresse and J. Furthmüller, *Phys. Rev. B*, 1996, **54**, 11169-11186.
- 4 J. P. Perdew, K. Burke and M. Ernzerhof, *Phys. Rev. Lett.*, 1996, **77**, 3865.
- 5 W. Chen, D. V. Semenok, I. A. Troyan, A. G. Ivanova, X. Huang, A. R. Oganov and T. Cui, *Phys. Rev. B*, 2020, **102**, 134510.
- 6 F. Porsch and W. B. Holzapfel, *Phys. Rev. Lett.*, 1993, **70**, 4087-4089.
- 7 Y. Ma, A. R. Oganov, Z. Li, Y. Xie and J. Kotakoski, *Phys. Rev. Lett.*, 2009, **102**, 065501.
- 8 C. J. Pickard and R. J. Needs, *Phys. Rev. Lett.*, 2009, **102**, 125702.
- 9 H. Katzke and P. Tolédano, *Phys. Rev. B*, 2008, **77**, 024109.
- 10 P. Tsuppayakorn-Aek, W. Luo, R. Ahuja and T. Bovornratanaraks, *Sci. Rep.*, 2018, **8**, 1-6.
- 11 A. D. Becke and K. E. Edgecombe, *J. Chem. Phys.*, 1990, **92**, 5397-5403.
- 12 S. Baroni, S. de Gironcoli, A. Dal Corso and P. Giannozzi, *Rev. Mod. Phys.*, 2001, **73**, 515-562.
- 13 A. Togo, F. Oba and I. Tanaka, *Phys. Rev. B*, 2008, **78**, 134106.
- 14 P. Giannozzi, S. Baroni, N. Bonini, M. Calandra, R. Car, C. Cavazzoni, D. Ceresoli, G. L. Chiarotti, M. Cococcioni, I. Dabo, A. Dal Corso, S. de Gironcoli, S. Fabris, G. Fratesi, R. Gebauer, U. Gerstmann, C. Gougoussis, A. Kokalj, M. Lazzeri, L. Martin-Samos, N. Marzari, F. Mauri, R. Mazzarello, S. Paolini, A. Pasquarello, L. Paulatto, C. Sbraccia, S. Scandolo, G. Sclauzero, A. P. Seitsonen, A. Smogunov, P. Umari and R. M. Wentzcovitch, *J. Phys.: Condens. Matter*, 2009, **21**, 395502.
- 15 P. B. Allen and R. C. Dynes, *Phys. Rev. B*, 1975, **12**, 905-922.
- 16 J. Carbotte, *Rev. Mod. Phys.*, 1990, **62**, 1027.
- 17 P. B. Allen and B. Mitrović, *Solid State Phys.*, 1983, **37**, 1-92.
- 18 M. Ghezali, B. Amrani, Y. Cherchab and N. Sekkal, *Mater. Chem. Phys.*, 2008,

**112**, 774-778.

19 A. Kulkarni, J. C. Schön, K. Doll and M. Jansen, *Chem. - Asian J.*, 2013, **8**, 743-754.

20 S. B. Schneider, D. Baumann, A. Salamat and W. Schnick, *J. Appl. Phys.*, 2012, **111**, 093503.

21 G. Vaitheeswaran, V. Kanchana and M. Rajagopalan, *Solid State Commun.*, 2002, **124**, 97-102.

22 S. Ono, K. Nomura and H. Hayakawa, *J. Less-Common Met.*, 1974, **38**, 119-130.

23 H. G. v. Schnering, W. Wichelhaus and M. S. Nahrup, *Z. Anorg. Allg. Chem.*, 1975, **412**, 193-201.

24 X. Chen, L. Zhu and S. Yamanaka, *J. Solid State Chem.*, 2003, **173**, 449-455.

25 W. Wichelhaus and S. HGv, *Naturwiss.*, 1975, **62**, 180.

26 Y. Zhou, L.-T. Shi, A. K. Liang, Z.-Y. Zeng, X.-R. Chen and H.-Y. Geng, *RSC Adv.*, 2021, **11**, 3058-3070.

27 G. Vaitheeswaran, V. Kanchana and M. Rajagopalan, *J. Alloys Compd.*, 2002, **336**, 46-55.

28 H. Xiao, Y. Dan, B. Suo and X. Chen, *J. Phys. Chem. C*, 2020, **124**, 2247-2249.

29 R. F. W. Bader, *Acc. Chem. Res.*, 1985, **18**, 9-15.

30 J. Kortus, I. I. Mazin, K. D. Belashchenko, V. P. Antropov and L. L. Boyer, *Phys. Rev. Lett.*, 2001, **86**, 4656-4659.